Supporting information for

Thermal stability and dynamics of soft nanoparticle membranes: role of entropy, enthalpy and membrane compressibility.

Nimmi Das A [a], Nafisa Begam [b], Sivasurender Chandran [c], Aparna Swain [a], Michael Sprung [d], and J. K. Basu[a,*]

[a] Department of Physics, Indian Institute of Science, Bangalore, 560012, India.

[b] Institute of Applied Physics, University of Tuebingen, 72076 Tuebingen, Germany.

[c] Institute of Physics, University of Freiburg, 79104 Freiburg, Germany.

[d] Deutsches Elektronen Synchrotron DESY, Notkestresse 85, 22607 Hamburg, Germany.

[*] E-mail: basu@iisc.ac.in

This document complements the main text by discussing the details of the sample preparation, their characterization, and the estimation of the radial distribution function from the micrographs obtained from transmission electron microscopy (TEM) and atomic force microscopy (AFM). Also discussed are the X-ray photon correlation spectroscopy (XPCS) based wave-vector and temperature dependent microscopic dynamics underlying the structural disordering of the membranes.

1. **Sample preparation:**

All experiments were carried out on ultra-thin layer of polystyrene grafted gold nanoparticles (PGNPs). PGNPs were synthesized through a modified grafting-to-method as given in the literature[1–3].

I. Characterization of PGNPs

As synthesized PGNPs were dried under vacuum, to remove any traces of solvent, and characterized through a palette of techniques to measure their overall size, core size, density of grafted polymers, and the glass transition temperature of the respective membranes. Transmission Electron Microscopy (TEM) images used to deduce the core sizes of PGNPs with different graft molecular weights $M_w = 3\,\text{kDa}$, $20\,\text{kDa}$, and $53\,\text{kDa}$ are shown Figure S1(a)-(d). The distribution of the core sizes of respective PGNPs were shown in the insets.

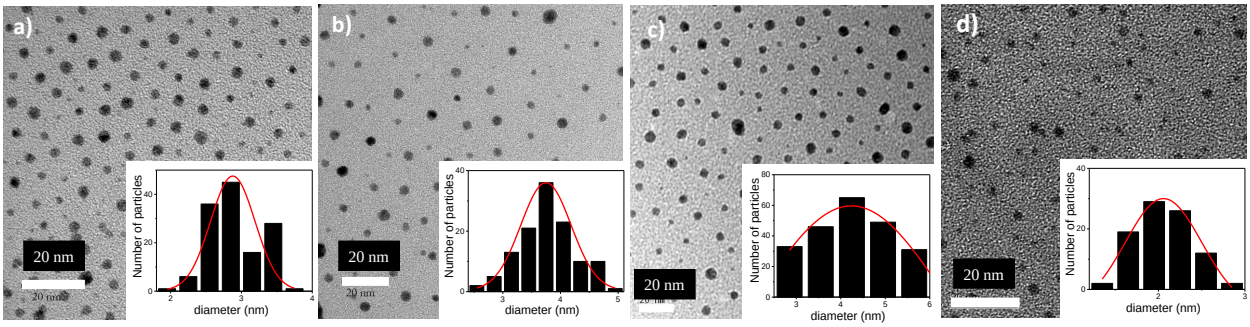

Figure S1: TEM images of PGNPs- a) S, b) M, c) M-low σ and d) L. Inset gives size distribution of the nanoparticle core.

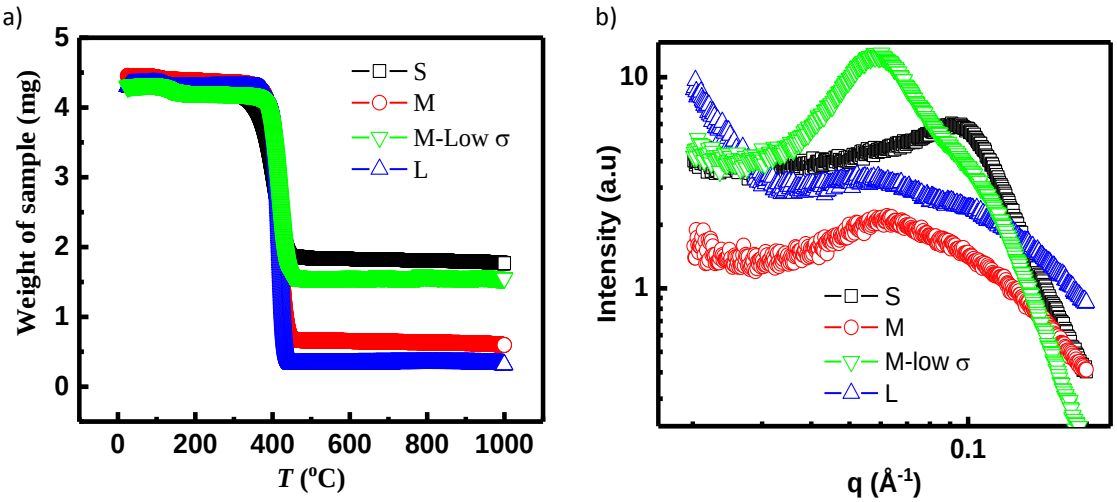

Figure S2: a) Mass vs temperature thermograph and b) Intensity vs wave vector profiles of all PGNPs. All symbols are defined in respective panels

Thermogravimetric analysis (TGA) (Figure S2(a)) was performed to deduce the mean weight fraction of Au core and PS corona in the PGNPs. Grafting density of PGNPs were calculated using Au fraction from TGA and core size from TEM. We used small angle X-ray scattering SAXS (Bruker, Nanostar Germany) to measure the overall PGNP size combining both the core and the polystyrene shell. SAXS profiles (intensity vs wave vector) of powder samples of different PGNPs, shown in (Figure S2(b)) captures the structure factor peak characterizing the mean separation between two neighboring PGNPs, which is equivalent to the diameter of the PGNP in powder form. Glass transition temperature (T_g) of PGNPs were measured using differential scanning calorimetry (DSC) (refer Figure S3). Bulk T_g of polymer substrates are also calculated using DSC as given in the references[3]. Defining characteristics of PGNPs, as obtained, are summarized in Table 1 and 2 of the main text.

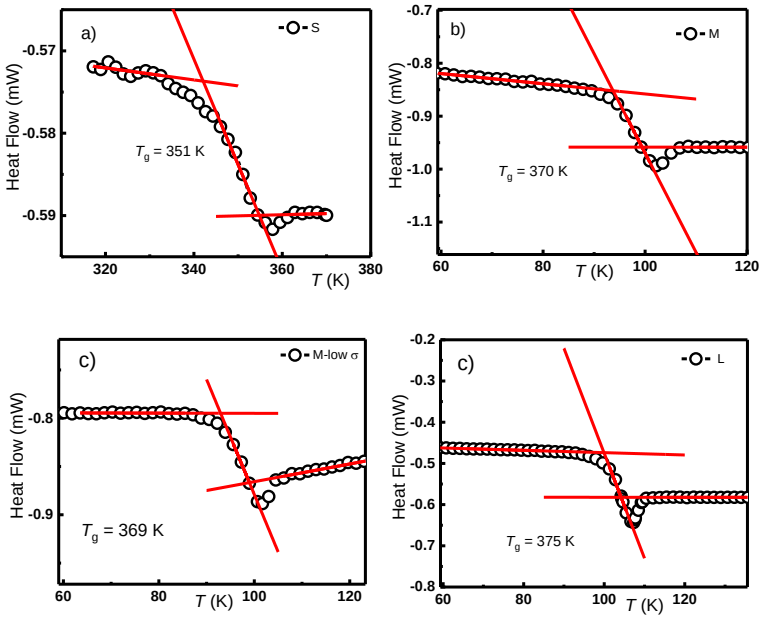

Figure S3: Bulk T_g determination of PGNP- a) S, b) M and c) M-lowσ, d) L from DSC curves using 3 slope method. Red straight lines trace the different slopes on DSC curves allowing to visualize the T_g of respective samples.

II. Preparation of supported PGNP membranes

As described in the main text, PGNPs membranes, self-assembled on air-water interface, were transferred onto three different substrates viz. silicon (Si), polystyrene (PS), poly (tert-butyl acrylate) (PtBA). Here, we describe the preparation of the respective substrates.

- Si substrate: Si wafer was cleaned in fuming piranha solution followed by dipping in a diluted HF bath (water : HF = 50:1). During piranha treatment all organic residues on the substrate were removed, leaving a thin native SiO_2 layer. Such native SiO_2 layer was etched by dipping in HF bath to obtain clean hydrophobic Si.
- PS and PtBA substrate: PS or PtBA films of a given thickness were spin-coated (Apex Instrument, India) from a homogeneous solution of the respective polymers in toluene, on a freshly treated Si with a native oxide layer of thickness *ca.*1 nm. Subsequently, PS and PtBA films were respectively annealed at 145 °C (T_g = 100 °C) and 70 °C (T_g = 38 °C) under vacuum of 5×10^{-5} mbar for 12 hours during which preparation-induced stresses are expected to relax.

  Thickness of the as coated films (substrates) were measured using X-ray reflectivity (Rigaku SmartLab instrument with X-ray beam of Cu K_α) (Fig S4). Thickness of PS20k, PS50k,

PS100k, PS400k and PtBA are 89 nm, 83 nm, 85 nm, 75 nm and 80 nm respectively. All films were made purposefully thicker to avoid any possible confinement effects.

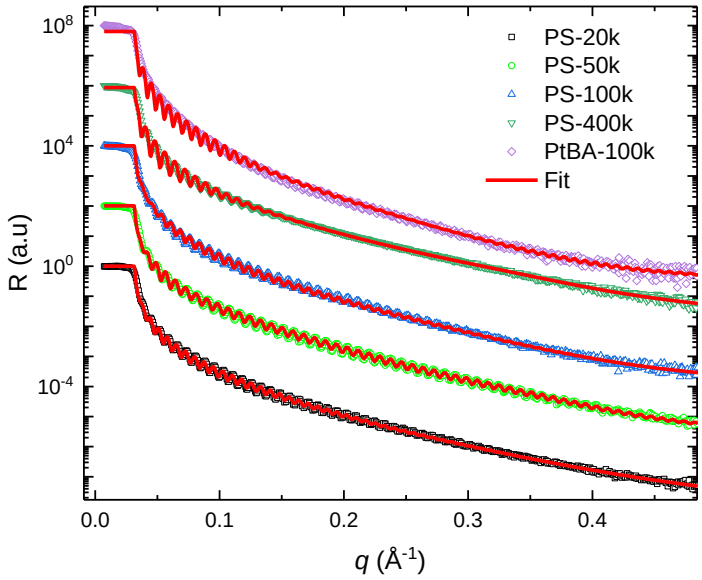

Figure S4: X-ray reflectivity profiles (symbols) of all films are shown along with the respective fits (red curve). All symbols are defined in the panel.

Monolayer of PGNPs was created at the air-water interface in a Langmuir-Blodgett (LB) trough (KSV NIMA) using the following procedure. 110 µl of homogeneous solution of PGNPs ($0.5\,\mathrm{g\,l^{-1}}$) in chloroform was spread on the water surface using a Hamilton syringe. Monolayer of connected granules of PGNPs were formed upon the rapid evaporation of solvent[4]. A dense film of PGNPs was obtained after compression of the monolayer to a surface pressure of $35\,\mathrm{mN\,m^{-1}}$, which was subsequently transferred on to a substrate through horizontal dipping method (Langmuir-Schaefer method). Surface morphology of PGNP membranes were visualized using atomic force microscopy (AFM) (Figure S5) and the extent of order in each sample was captured by the respective pair correlation functions (insets of Figure S5 (a)-(d)). Further, we quantified the size distribution of PGNP grains by histograms.

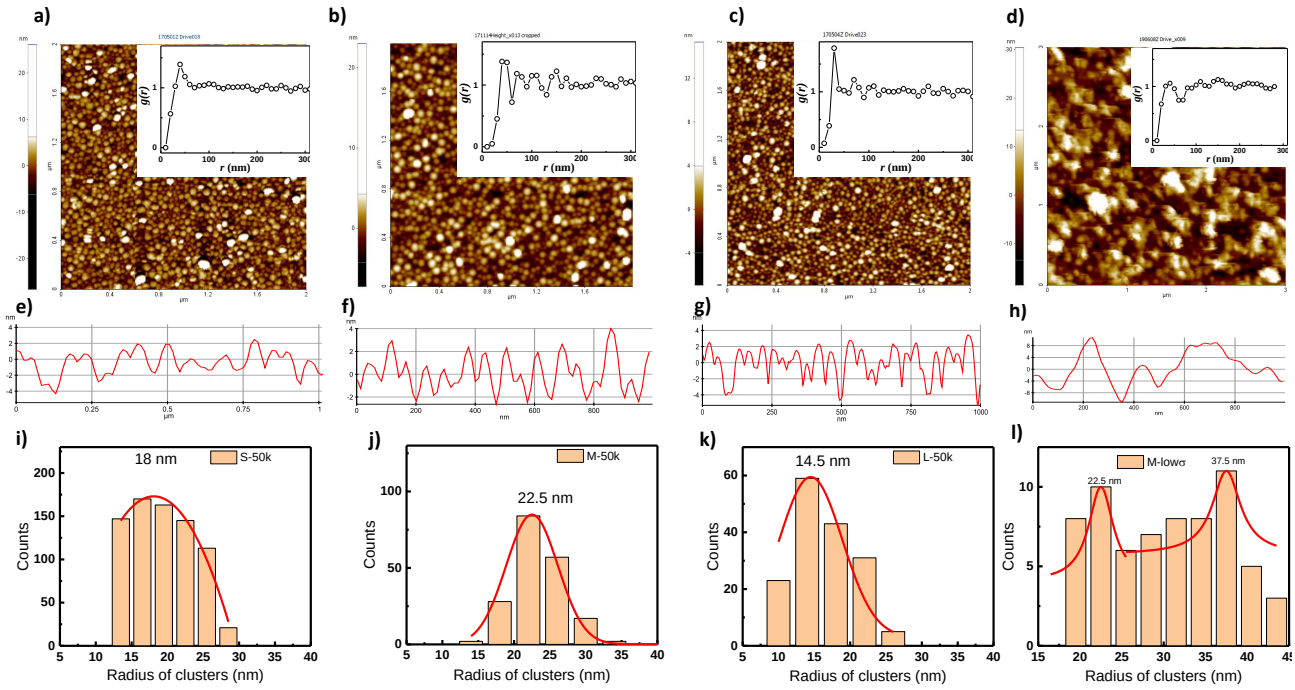

Figure S5: AFM micrographs of a) S-50k, b) M-50k, c) L-50k, and d) M-lowσ on silicon substrate. The corresponding calculated grain pair correlation function, $g(r)$ is given in inset and corresponding height profiles are given in e), f), g), and h). The histograms, corresponding to images (a)–(d), capturing the size distribution of grains are shown in (i)-(l).

In Figure S6, we show the isothermal compression modulus of L membranes transferred on different substrates, which are used for XPCS measurements. The extracted values of K_{f} are reported in Table S1.

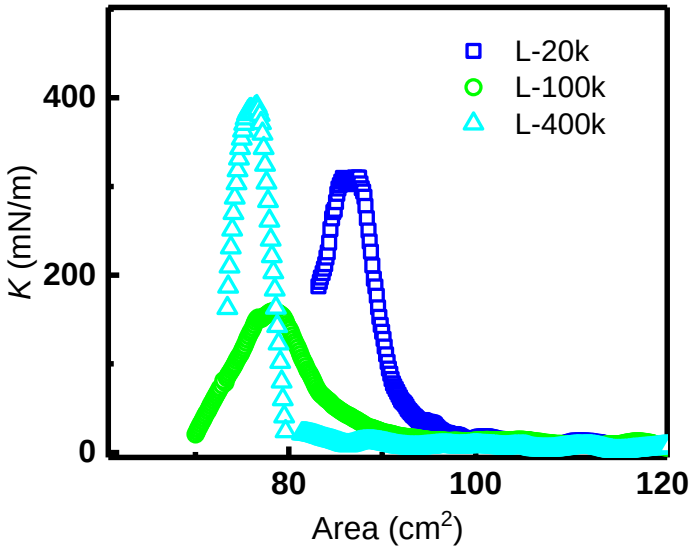

Figure S6: Isothermal compression modulus (K) of L membranes deposited on various PS substrates, used for XPCS measurements.

Table S1: Isothermal compression modulus at the final transfer pressure

Sample	K_f ($mN\,m^{-1}$)
L-20k	147
L-50k	143
L-100k	20
L-400k	163

2. Structural disordering captured using AFM

In-situ AFM imaging was employed to track temperature driven structural disorder in PGNP membranes. Temperature dependent structural disordering of L-50k is shown in Figure S7.

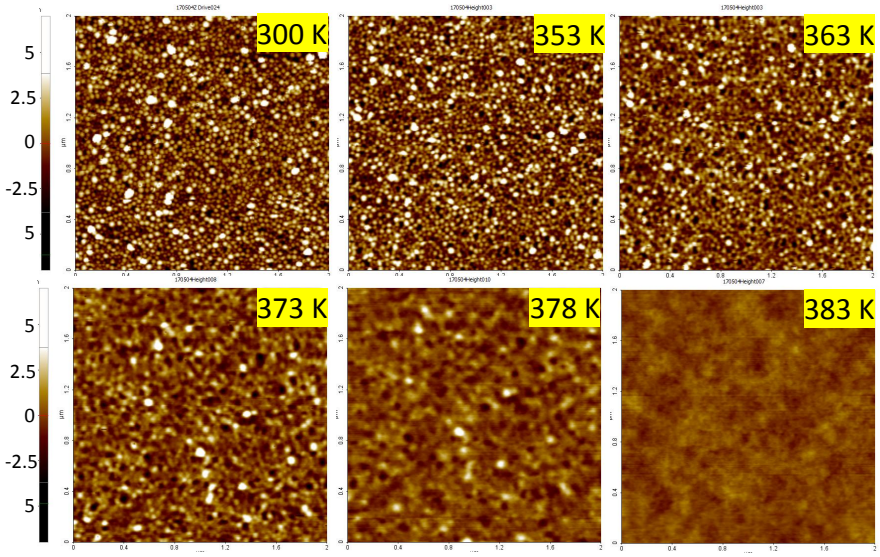

Figure S7: AFM surface topography of L-50k at different temperatures, as mentioned in respective images.

Interplay of entropic interaction, between grafted and substrate polymers, and membrane flexibility on membrane disordering is illustrated by comparing AFM images and corresponding $g(r)s$ of different membranes at various temperatures as shown in Figure S8.

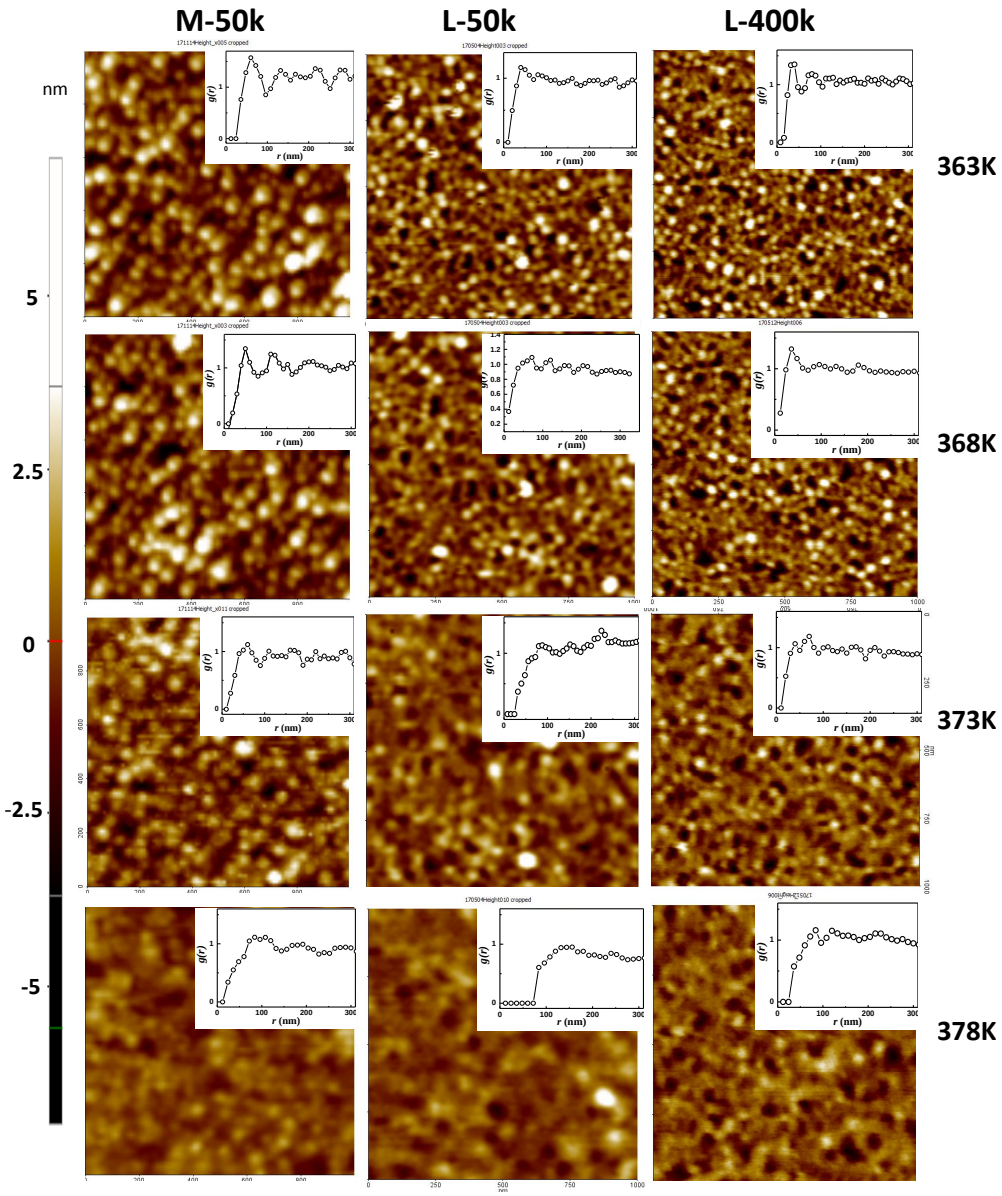

Figure S8: Temperature driven structural disordering of various membranes on PS substrates captured using AFM. Columns left to right corresponds to M-50k, L-50k and L-400k samples respectively. Ordering of M-50k, L-50k and L-400k at a fixed temperature is compared across the rows. Temperatures corresponding to the images are mentioned in the figure. Calculated $g(r)$ of the respective images are shown in the inset of each image.

3. Change in the PGNP height profile as a function of temperature

We have calculated the average height of PGNP grains at two temperatures for L-PtBA sample (Figure S9) from AFM images. As depicted in the Figure S9, the average surface height of the initially ordered configuration reduces from 7.7 nm to 5.7 nm by increasing temperature from 303 K to 318 K. However, during this process the grains retain their shape (Figure S9b). This indicates that the grains are vertically diffused into the underlying PtBA matrix without any grain fusion. Schematic shown in Figure S9c depicts difference in the height (h) of PGNP grains

during the transition (granular state to vertically diffused state).

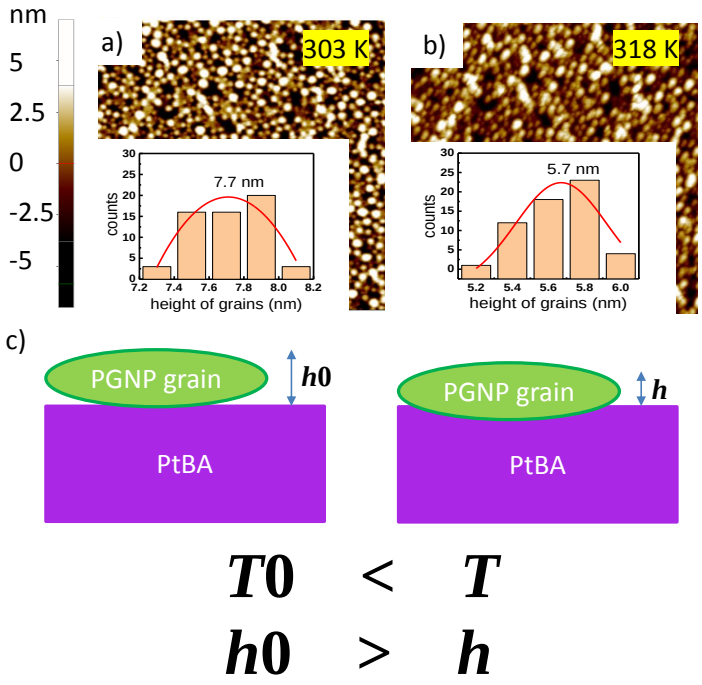

Figure S9: AFM surface topography of L-PtBA (a and b) at different temperatures, as mentioned in respective images. The size of AFM images is 2 μ x 2 μ. The inset shows the histogram of height of PGNP grains. c) Schematic showing the vertical diffusion of PGNP grains into PtBA substrate with an increase in temperature.

4. **Estimation of pair correlation function** $g(r)$

Pair correlation function measures how particle density varies radially from a reference particle. Calculation of $g(r)$ from a typical image with dense particle distribution is done in two steps,

(a) Locating the position of the grains. Figure S10 (a) depicts AFM image of a PGNP membrane. The image analyzing software ImageJ was used to find the center of grains as shown in Figure S10 (b).

(b) Randomly choosing a reference grain (see Figure S10 (c)). The number of particles in each annular ring of width dr is counted. Using the following equation, $g(r)$ is evaluated using a MATLAB code.

Two dimensional pair correlation function given by,

$$g(r) = \frac{1}{2\pi r\, dr}\frac{1}{n1\,\rho}\sum_{i=1}^{n}\sum_{j\neq i}^{n}\langle\delta(r-|r_j-r_i|)\rangle, \tag{1}$$

where n is the total number of particles, $n1$ is the total number of particles taken as center particle while counting, $\rho = \frac{n}{x^2}$ is the number density, and x^2 is the image size.

Calculated $g(r)$ is shown in Fig S10(d), where first peak indicates the inter-grain distance.

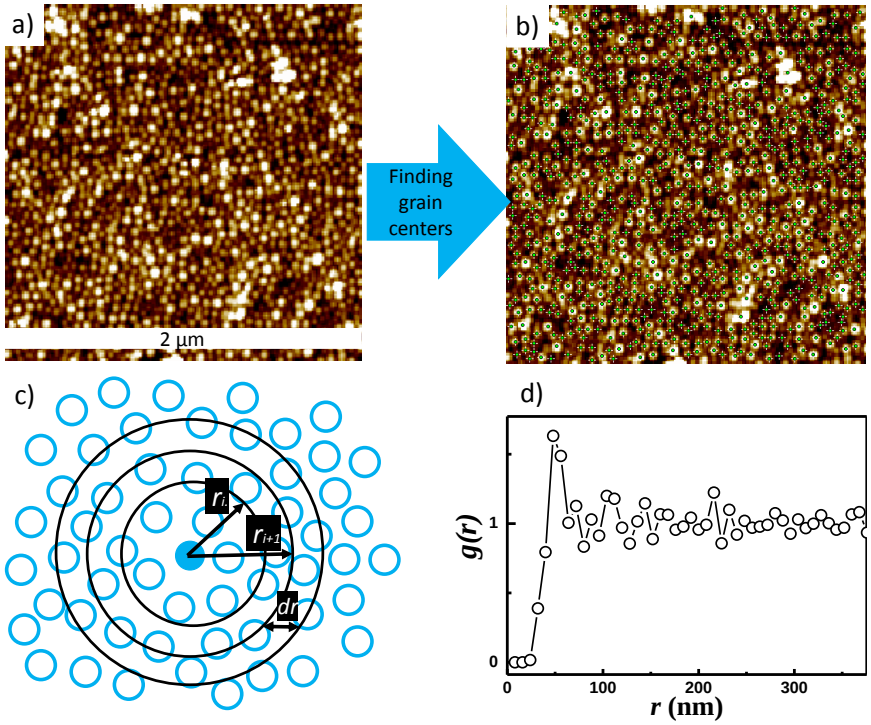

Figure S10: a) Typical AFM image of granular PGNP membrane, b) Center of grains are determined using ImageJ software, green plus symbol indicates the grain center. c) Schematic explaining $g(r)$ calculation, d) $g(r)$ calculated for panel (a) using definition in Equation (1).

5. PGNP distribution within a membrane

To see the distribution of Au cores (equivalent to distribution of PGNPs) inside the grains, TEM imaging was employed. Monolayer of PGNP (from water surface) was transferred at a low pressure 25 mN m^{-1} onto carbon coated copper grids for TEM measurements. The pair correlation function $g(r)$ quantifies the extent of ordering of individual PGNPs inside the grains. Figure S11(d) shows the $g(r)$ of as transferred PGNP film (before structural disordering of the grains) and disordered state (after the transition). First sharp peak at $r = 6$ nm corresponds to inter-nanoparticle distance inside the grains. The broad peak at 76 nm indicates the inter-grain distance in this loosely packed membrane. Disappearance of 76 nm peak could be witnessed, indicating the fusion of grains. Reduction in the intensity of 6 nm peak with temperature is the indication of individual particle fluctuation within and between the grains.

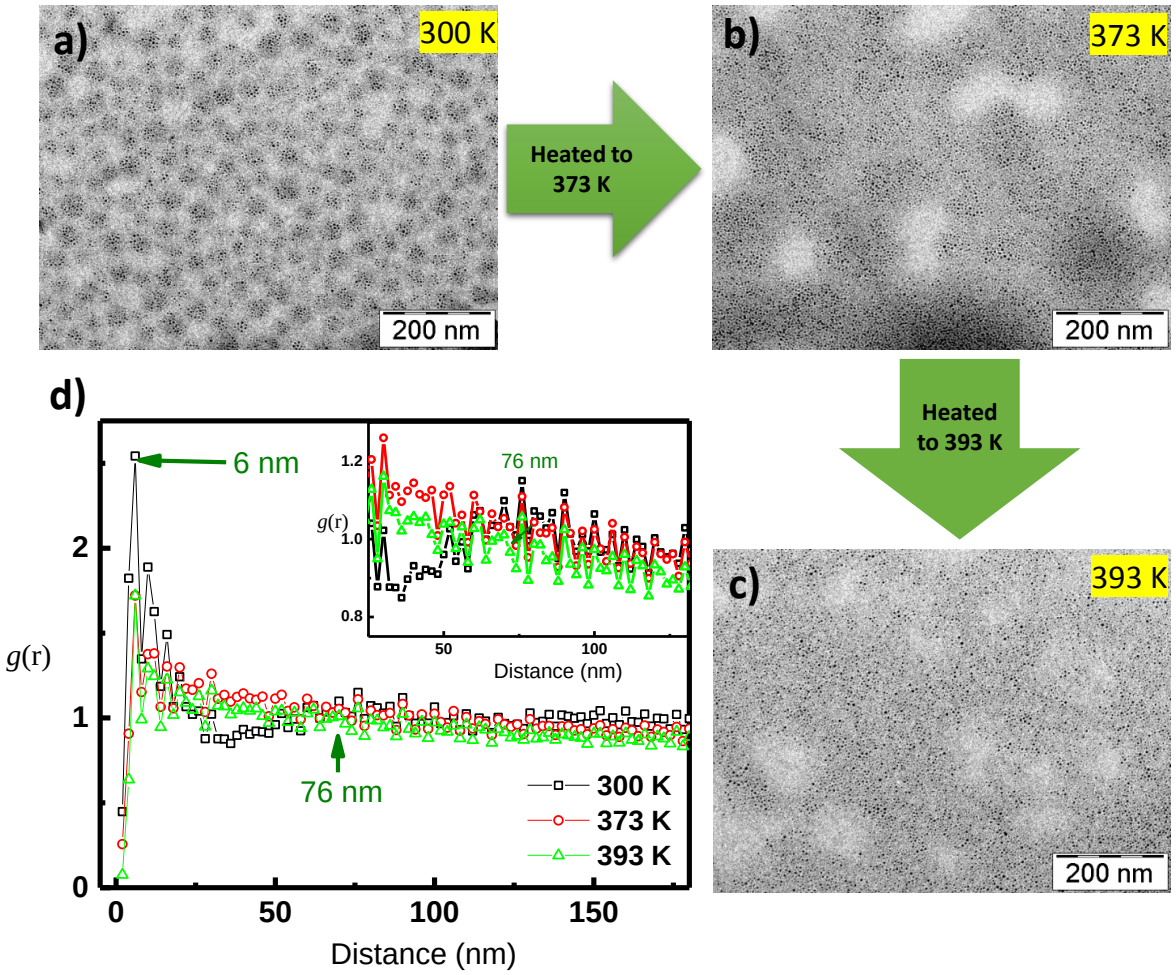

Figure S11: TEM images of S membrane transferred on copper grid at $\Pi = 25\,\mathrm{mN\,m^{-1}}$ (membrane was transferred at a lower surface pressure to clearly see individual grains). a) As-transferred membranes at room temperature, and the same membrane heated to b) 373 K, and c) 393 K. d) Calculated $g(r)$ of the gold cores at all temperatures. Inset shows enlarged peak at $r = 76$ nm.

6. Study of microscopic dynamics using XPCS

Synchrotron based X-ray photon correlation spectroscopy (XPCS) measurements on PGNP/PS and PGNP/PtBA samples were performed at the beamline P10, PETRA III, DESY, Hamburg, Germany. Incident X-ray beam of energy 8 keV and beam size 25 × 25 μm^2 was used to probe the dynamics of PGNP membranes at various temperatures. Time series of scattered intensity was collected using Lambda detector. Total exposed area of the detector was 84.5 x 28.2 mm^2 (area 1536 × 512 px^2, pixel size = 55 × 55 μm^2)[3,5]. A typical scattering data from the area detector is shown in Figure S12.

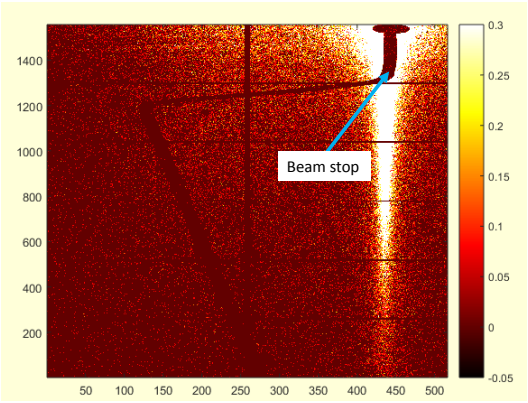

Figure S12: Typical X-ray scattering data collected using Lambda detector (sample: S-50k, T = 333 K).

Any traces of radiation damage in samples during XPCS measurements were verified by comparing total scattering intensity from CCD images as a function of scan time. Total scattering intensity at two temperatures of M-50k ans S-PtBA samples are shown in Figure S13. No appreciable increase or decrease in total intensity during the measurement period indicates absence of radiation induced damages.

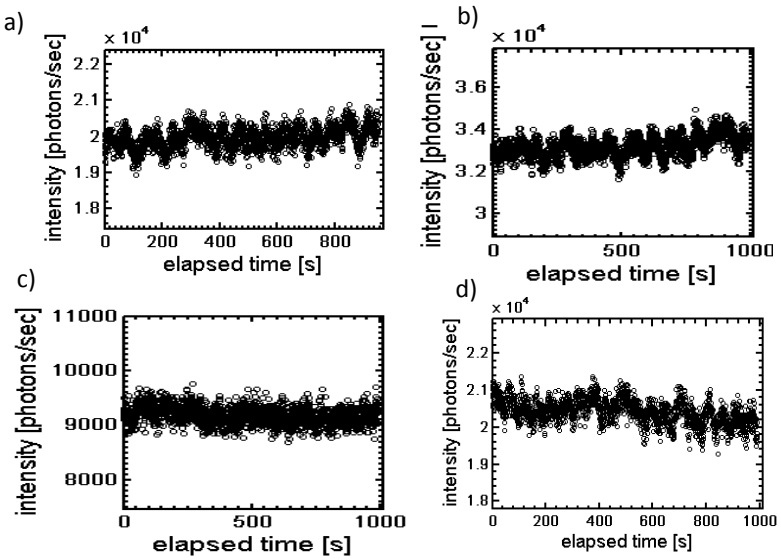

Figure S13: Variation of total scattering intensity from CCD images with time for M-50k at a) T = 333 K, b) T = 363 K and for S-PtBA at a) T = 280 K, b) T = 300 K.

Data reduction and analysis were performed using MATLAB based package (XPCSGUI) developed by P10 (Petra III, DESY, Germany). Time correlation function, $g_2(q_x, t)$ of scattered

intensity $I(q_x, t)$ at different q-regions were calculated. Mathematically, $g_2(q_x, t)$ is defined as,

$$g_2(q_x, t) = \frac{\langle I(q_x, t)\rangle \langle I(q_x, t + \delta t)\rangle}{|I(q_x, t)|^2}, \tag{2}$$

Intermediate scattering function (ISF) (Figure S14), $F(q_x, t)$ is related to $g_2(q_x, t)$ by the following relation,

$$g_2(q_x, t) = 1 + b\ |F(q_x, t)^2|, \tag{3}$$

where b is an instrumental factor called the speckle contrast and t is delay time. $F(q_x, t)$ has the general time dependent exponential functional form,

$$F(q_x, t) = exp\left[-(t/\tau)^{\beta}\right]\Big|_{q_x}, \tag{4}$$

where τ and β are the characteristic relaxation time and Kohlrausch exponent, respectively. Extracted τ and β for all the samples as a function of q_x are given in Figure S15 and Figure S16, respectively. All ISFs followed a compressed exponential decay with $\beta > 1$.

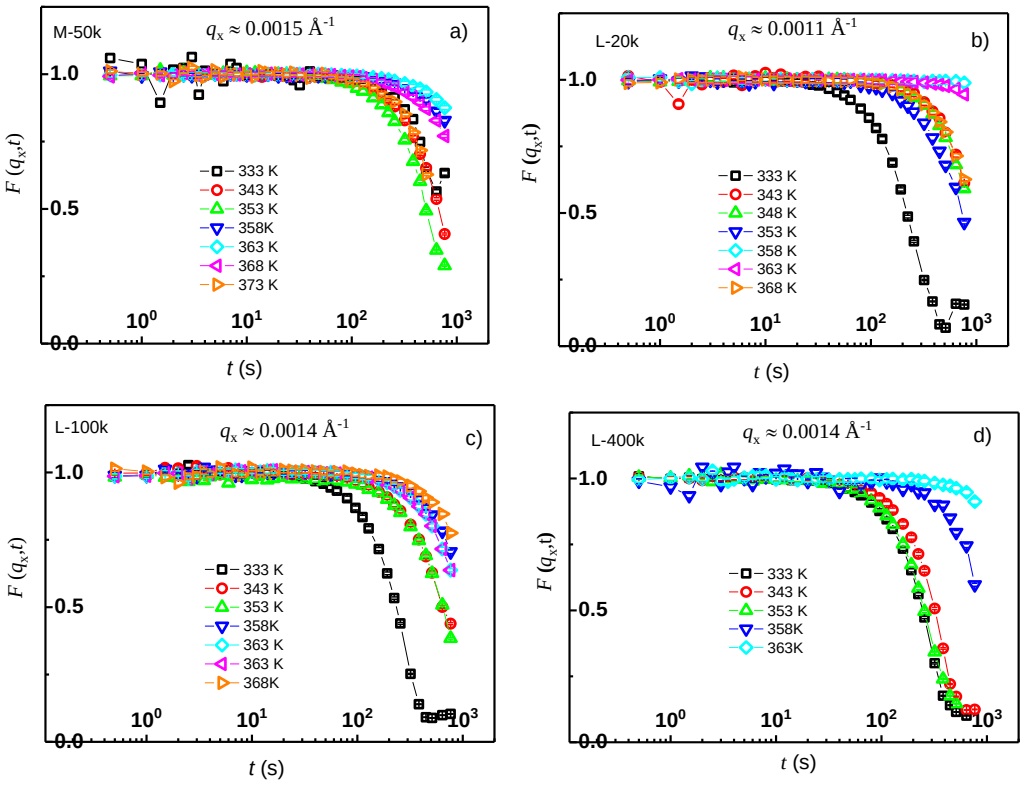

Figure S14: Temperature dependence of ISFs of a) M-50k, b) L-20k, c) L-100k, d) L-400k samples. Corresponding temperatures and q_x values are indicated in the respective panels.

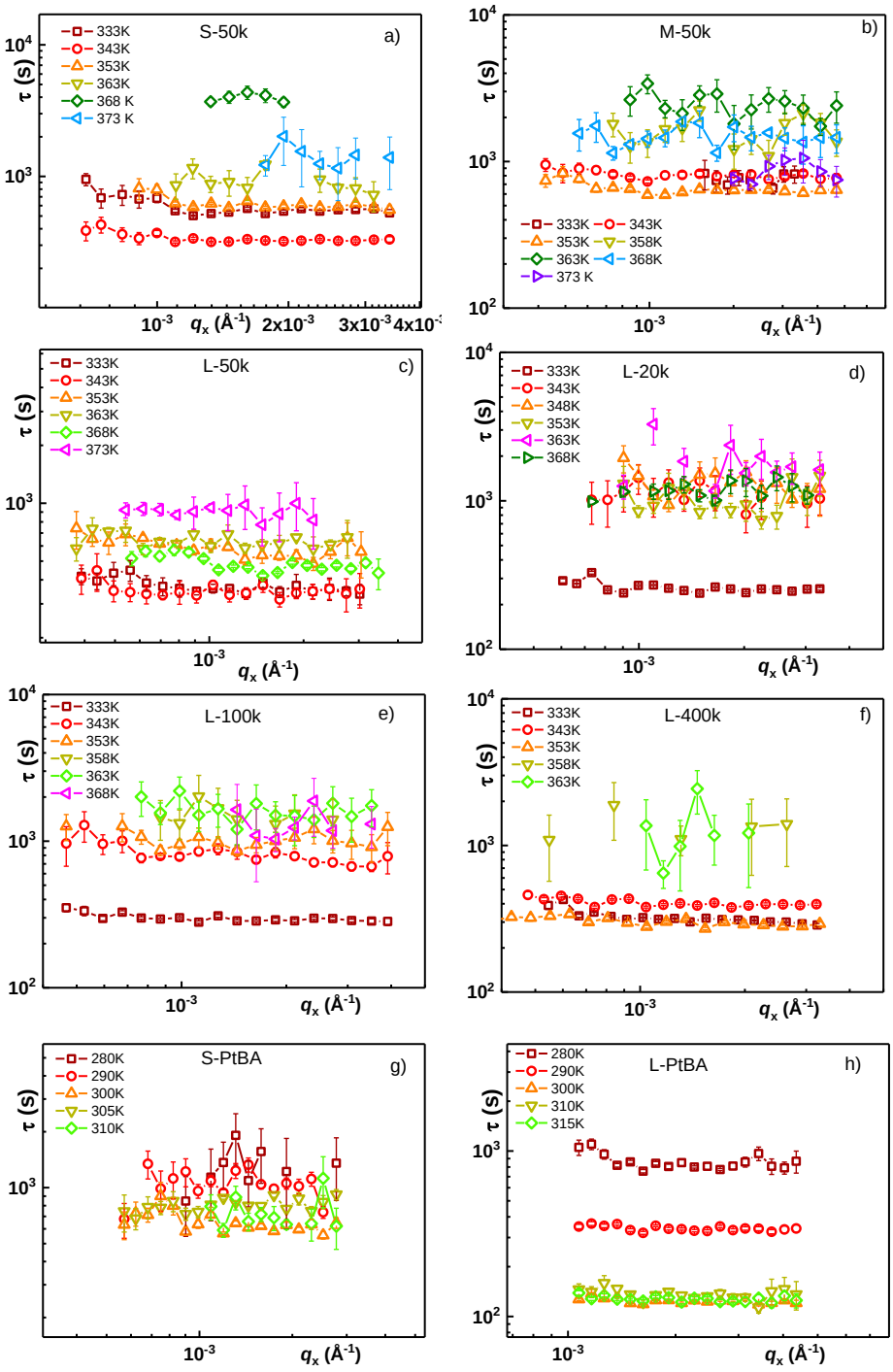

Figure S15: Temperature dependent relaxation time extracted from ISFs using Equation (4) for samples a) S-50k, b) M50k, c) L-50k, d) L-20k, e) L-100k, f) L-400k, g) S-PtBA and h) L-PtBA.

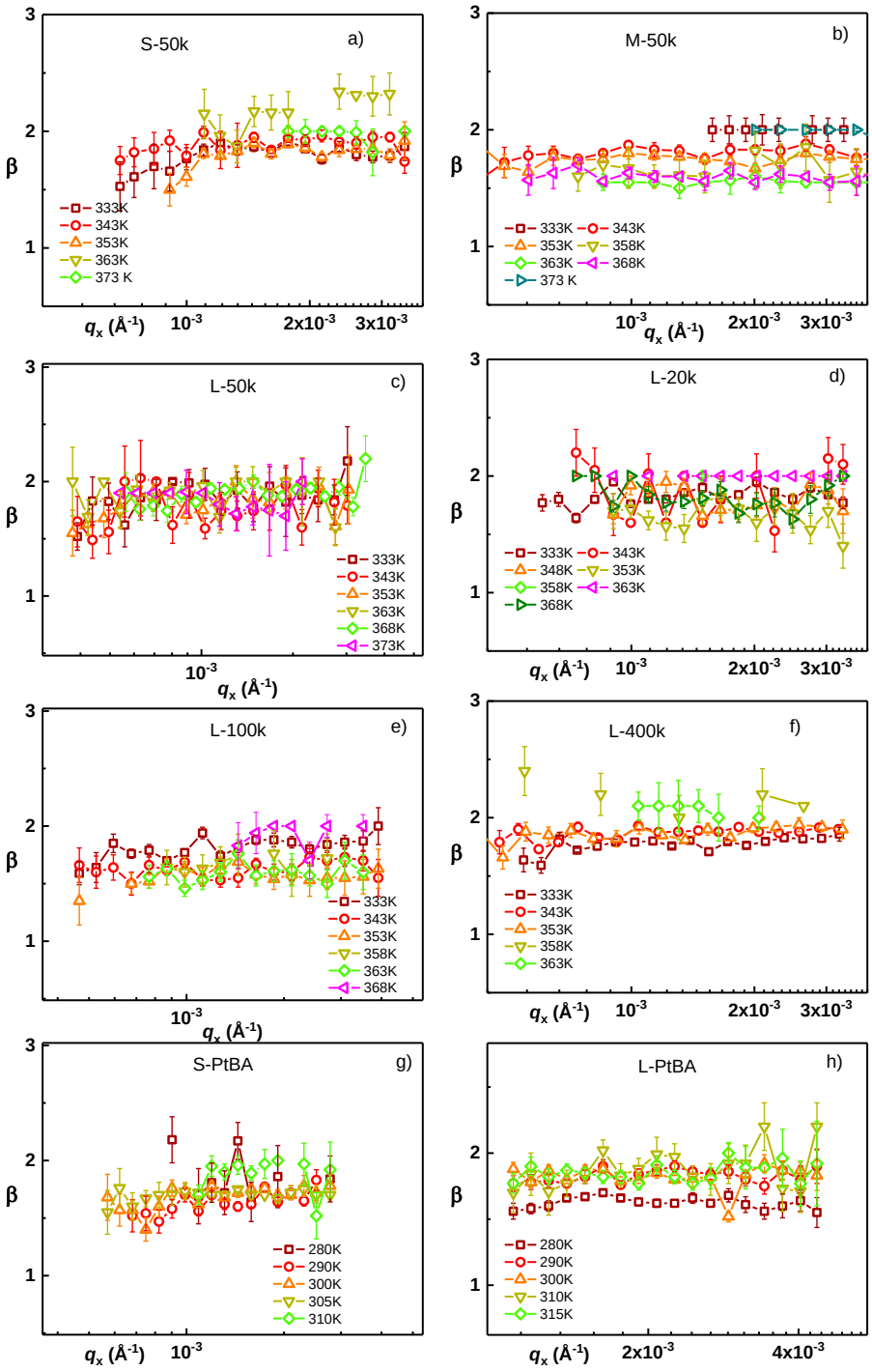

Figure S16: Kohlrausch exponent β used for modeling ISFs using Equation (4) at different temperatures for samples a) S-50k, b) M-50k, c) L-50k, d) L-20k, e) L-100k, f) L-400k, g) S-PtBA and h) L-PtBA.

7. Diffusive dynamics observed at high temperature

At elevated temperatures (i.e., above T_g of both the membrane and substrate), membranes were completely disordered and formed a homogeneous layer. ISFs of PGNP/PS samples exhibited two exponential decays with two relaxation times as shown in Figure S17. One of the relaxation times is wave vector independent. Interestingly, the shorter relaxation time, τ_d shows a power

law dependence of $\approx q_x^{-2}$, which is indicative of diffusive dynamics of PGNPs (Fig. S17).

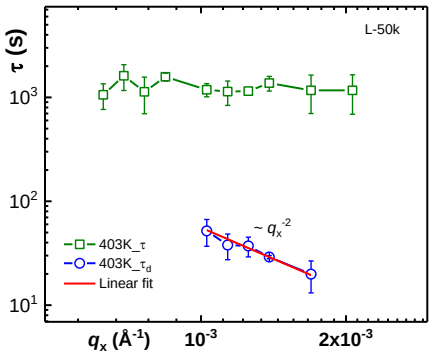

Figure S17: Wave vector dependent relaxation time of L-50k sample at $T = 403$ K. Two relaxation times were observed at this temperature. The power law dependence of relaxation time τ_d ($\approx q_x^{-2}$) is indicative of diffusive dynamics in the system.

References

[1] C. K. Yee, R. Jordan, A. Ulman, H. White, A. King, M. Rafailovich and J. Sokolov, *Langmuir*, 1999, **15**, 3486–3491.

[2] S. Chandran, N. Begam, V. Padmanabhan and J. K. Basu, *Nature Communications*, 2014, **5**, 3697.

[3] N. Begam, N. D. Anthuparambil, S. Chandran, M. Ibrahim, V. Padmanabhan, M. Sprung and J. K. Basu, *Soft Matter*, 2018, **14**, 8853–8859.

[4] C. Sarika, G. Tomar, J. K. Basu and U. Thiele, *Soft Matter*, 2015, **11**, 8975–8980.

[5] N. Begam, S. Chandran, M. Sprung and J. K. Basu, *Macromolecules*, 2015, **48**, 6646–6651.